Supporting Information

Revisiting the Origin of Nanopore Current Blockage for Volume Difference Sensing at the Atomic Level

Meng-Yin Li[†‡], Yi-Lun Ying[†‡], Jie Yu[⊥], Shao-Chuang Liu[†], Ya-Qian Wang[⊥], Shuang Li[⊥], and Yi-Tao Long*[†]

Affiliations:

[†]State Key Laboratory of Analytical Chemistry for Life Science, School of Chemistry and Chemical Engineering, Nanjing University, Nanjing 210023, P.R. China

[‡]Chemistry and Biomedicine Innovation Center, Nanjing University, Nanjing 210023, P.R. China

[⊥]School of Chemistry and Molecular Engineering, East China University of Science and Technology, Shanghai 200237, P.R. China

* E-mail: yitaolong@nju.edu.cn (to Y.T.L.)

Supporting Methods

Calculation of separation rate

The separation is defined as $R = 2(I_{C-A_3} - I_{mC-\ _3})/(W_{C-A_3} + W_{mC-A_3})$ based on our previous work[1]. In this definition, I_{C-A_3} and I_{mC-A_3} represents the mean residual current of C-A_3 and mC-A_3 based on the Gaussian fit (Figure S1), respectively, while the W_{C-A_3} and W_{mC-A_3} represents the peak width of Gaussian peak for residual current histogram of C-A_3 and mC-A_3, respectively.

Estimation of contribution fraction of non-covalent interaction to current change

As clarified in manuscript, the volume excluded by target molecule could centralize the ionic current sensing from the whole nanopore to the region where the molecule stays, which would help to enlarge the effects of interaction induced conductance change. Therefore, the blockage current is correlated to the product of volume exclusion effect and interaction effect. The estimated current blockage of target molecule can be revised as

$$\Delta I_b = -\frac{\sigma_0 \psi V}{h^2}\left[1 + f\left(\frac{d_m}{D_p}, \frac{l_m}{h}\right)\right] - \frac{(\sigma_0 - \sigma_1)\psi(V_0 - V)}{h^2}\left[1 + f\left(\frac{d_m}{D_p}, \frac{l_m}{h}\right)\right] \quad \text{(S1)}$$

where σ_0 and σ_1 are the nanopore solution conductivity of nanopore without and with the target molecule inside, respectively, V_0 represents the volume of the nanopore lumen, ψ is the transmembrane potential across the nanopore, h accounts for effective sensing length of the nanopore beyond physical limitation, V quantifies the volume of the target molecule, and $f(d_m/D_p,\ l_m/h)$ corrects the error induced by the relative geometry of the target molecule and the nanopore with d_m, D_p and l_m represents diameter of the molecule, diameter of the nanopore and the length of the molecule, respectively.

Thus, the residual current during a target molecule inside can be written as

$$I_{res} = \frac{\sigma_1 \psi(V_0 - V)}{h^2}\left[1 + f\left(\frac{d_m}{D_p}, \frac{l_m}{h}\right)\right] \quad \text{(S2)}$$

Since the volume of a methyl group is about 0.03 nm^3, an extra single methyl group that accounts for about 3.16% of the volume of C-A_3 (0.95 nm^3) induced about 6.43% current blockage enhancement. Based on equation (R3), with the correction term of relative geometry $f(d_m/D_p\ , l_m/h)$ considered to be same for C-A_3 and mC-A_3, the ration of residual current for C-A_3 and mC-A_3 can be simplified as

$$\frac{I_{C-A3}}{I_{mC-A3}} = \frac{\sigma_{C-A3}(V_0 - V_{C-A3})}{\sigma_{mC-A3}(V_0 - V_{mC-A3})} \quad \text{(S3)}$$

Therefore, compared to C-A_3, the mC-A_3 enhanced interactions result in a 5.63% decrease in conductance. Thus, the methylcytosine enhanced non-covalent effect contributed about 64.1% in total current change for mC-A_3 and C-A_3, while the extra volume of the methyl group is about 35.9%.

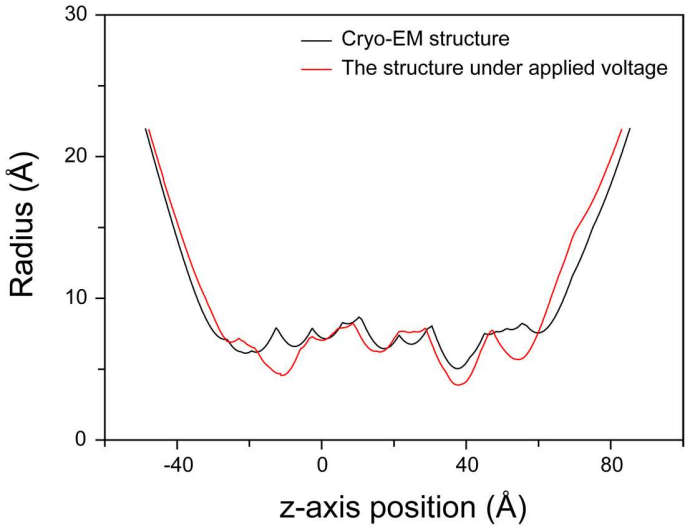

Figure S1. The radius of aerolysin lumen before and after the equilibrium under the applied voltage of +120 mV. The radius is calculated by HOLE program[2].

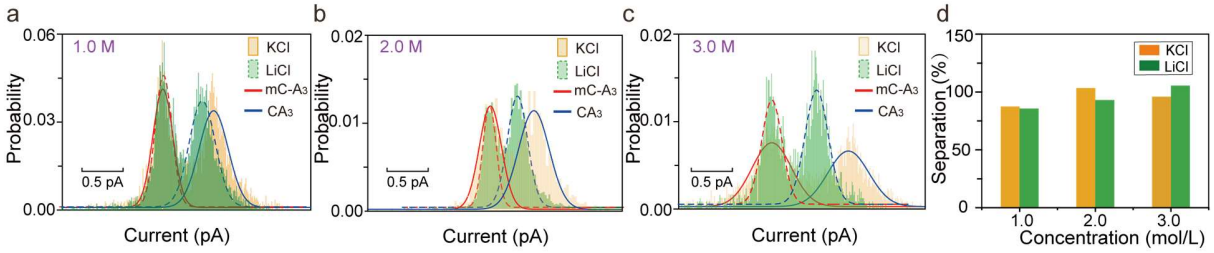

Figure S2. The current blockage histogram for the mixture of C-A_3 and mC-A_3 in KCl (orange) and LiCl (green) solution at the salt concentration of 1.0 M (a), 2.0 M (b) and 3.0 M (c). Current histograms are all fitted to two Gaussian peaks drawn as a solid line and dash line in KCl and LiCl, respectively. (d) Separation of the two current peaks corresponding to mC-A_3 and C-A_3 in KCl (orange) and LiCl (green) at 1.0 to 3.0 M salt concentration. All data were acquired in the presence of 2.0 μM at pH 8.0, 20 ± 2 °C.

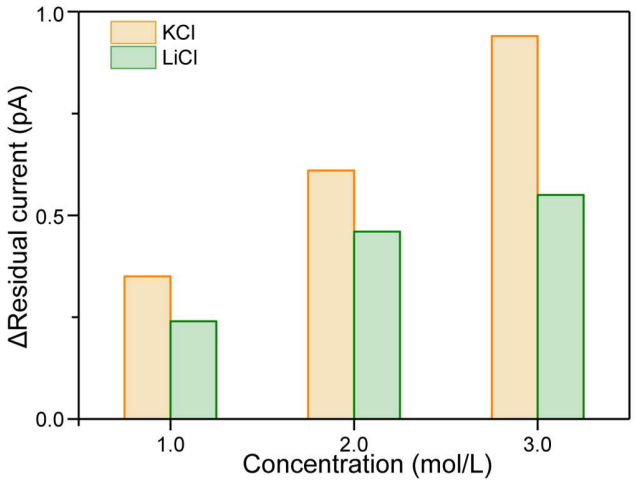

Figure S3. Residual current differences between mC-A_3 and C-A_3 in LiCl and KCl solution at different ionic strength. The C-A_3 were added into *cis* compartment when a single aerolysin nanopore was formed. After one hour, the same concentration mC-A_3 were added as well. ΔResidual current is defined as the difference between mC-A_3 and C-A_3 based on at least three experiments. ΔResidual current between the two populations of mC-A_3 and C-A_3 in LiCl are lower than those in KCl. The experiments were performed in 10 mM Tris, and 1 mM EDTA, pH 8.0 at +60 mV.

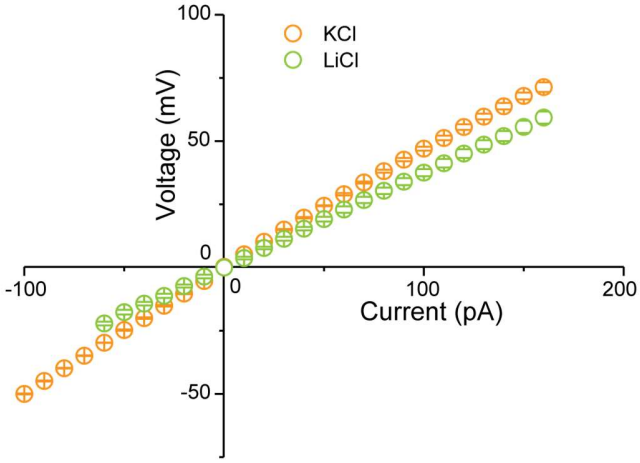

Figure S4. I-V curves for wild-type aerolysin nanopore in 1.0 LiCl and KCl solution. Experiments were performed in 10 mM Tris, and 1 mM EDTA, pH 8.0.

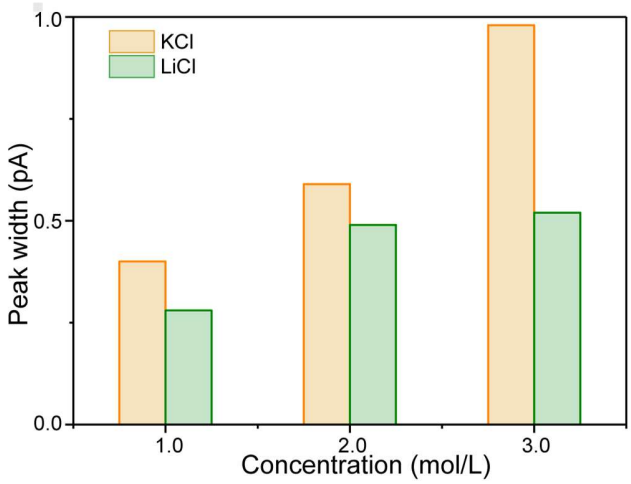

Figure S5. Peak width of mC-A$_3$ and C-A$_3$ in LiCl and KCl solution at different ionic strength. Oligomer C-A$_3$ were added into *cis* compartment when a single aerolysin nanopore was formed. After one hour, the same concentration mC-A$_3$ were added as well. The Gaussian peak widths of the ionic current histogram in LiCl are narrower than those in KCl. Experiments were performed in 10 mM Tris, and 1 mM EDTA, pH 8.0 at +60 mV.

Table S1. Mean values of event frequency for mC-A$_3$ and C-A$_3$ at different applied potentials. Values of event frequency (s^{-1}) were quantified as $f = 1/\tau_{on}$, where τ_{on} represents interval time. The standard deviation is based on at least three experiments.

Potential (mV)	Event Frequency (s^{-1})	
	mC-A$_3$	C-A$_3$
60	5.00 ± 0.00	6.00 ± 0.00
80	14.00 ± 0.00	14.00 ± 0.00
100	29.00 ± 3.00	25.00 ± 1.00
120	41.00 ± 2.00	38.00 ± 3.00
140	54.00 ± 3.00	49.00 ± 2.00
160	66.00 ± 2.00	58.00 ± 3.00

Table S2. Mean values of duration for mC-A$_3$ and C-A$_3$ at different applied potentials. Values were obtained by the fitted single exponential function to the duration histograms at each applied voltage. The standard deviation is based on at least three experiments.

Potential (mV)	Duration (ms)	
	mC-A$_3$	C-A$_3$

60	5.54 ± 0.17	4.72 ± 0.08
80	5.12 ± 0.14	3.90 ± 0.13
100	3.64 ± 0.16	2.93 ± 0.11
120	1.76 ± 0.10	1.37 ± 0.03
140	1.20 ± 0.08	0.94 ± 0.03
160	0.85 ± 0.06	0.66 ± 0.03

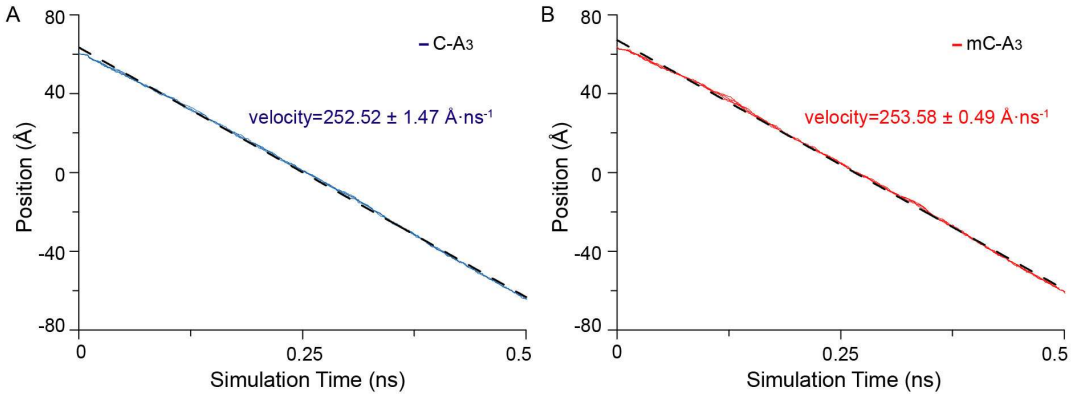

Figure S6. The position via simulation for C-A$_3$ (A) and mC-A$_3$ (B) with a constant velocity of 0.25 Å/ps during SMD simulation.

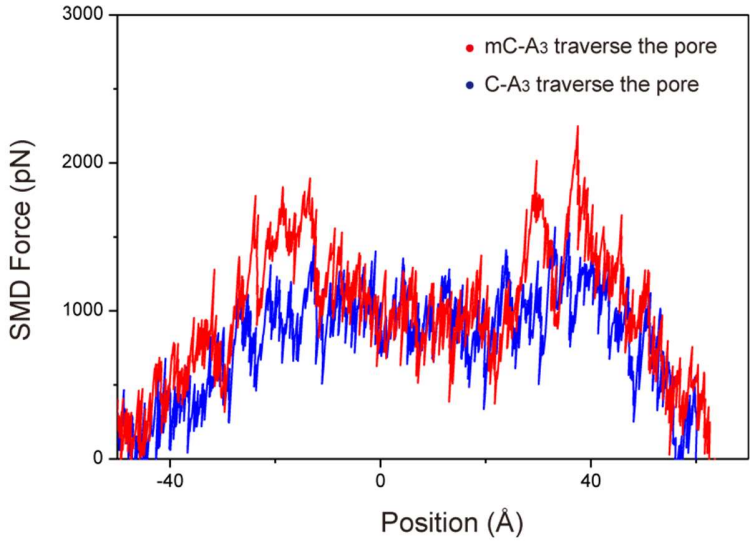

Figure S7. Steering force applied in the backbone of the mC-A$_3$ (red line) and C-A$_3$ (blue line) with a constant velocity of 0.10 Å/ps. SMD simulations were performed for the translocation of mC-A$_3$ (red line) and C-A$_3$ (blue line) through the pore with a constant velocity of 0.10 Å/ps.

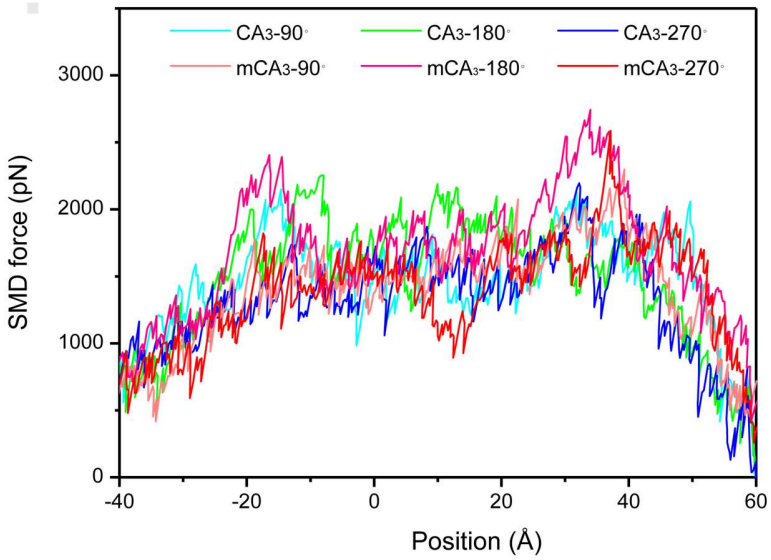

Figure S8. Steering force applied in the backbone of the mC-A$_3$ and C-A$_3$ with the initial conformation rotated at different degrees. SMD simulations were performed for the translocation of mC-A$_3$ and C-A$_3$ through the pore with a constant velocity of 0.25 Å/ps.

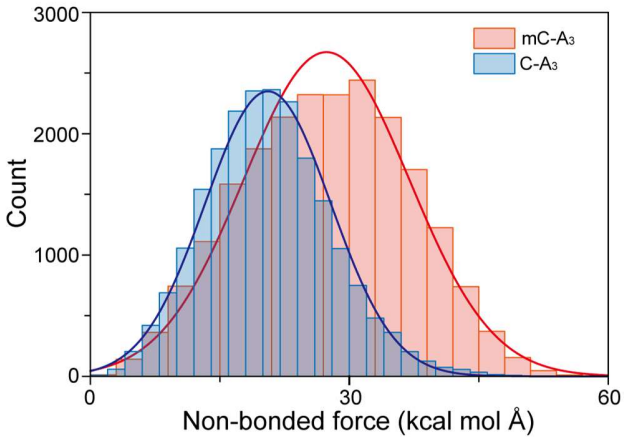

Figure S9. Non-bonded force exerted on mC-A$_3$ (red) or C-A$_3$ (blue) by all amino acid residues of aerolysin nanopore. The simulations were performed with the backbone of the two oligonucleotides restrained in R1 region of aerolysin. The non-bonded forces were calculated from the frames of the trajectories. The histograms of non-bonded force were fitted to the Gaussian distributions shown as red line and blue line for mC-A$_3$ and C-A$_3$, respectively.

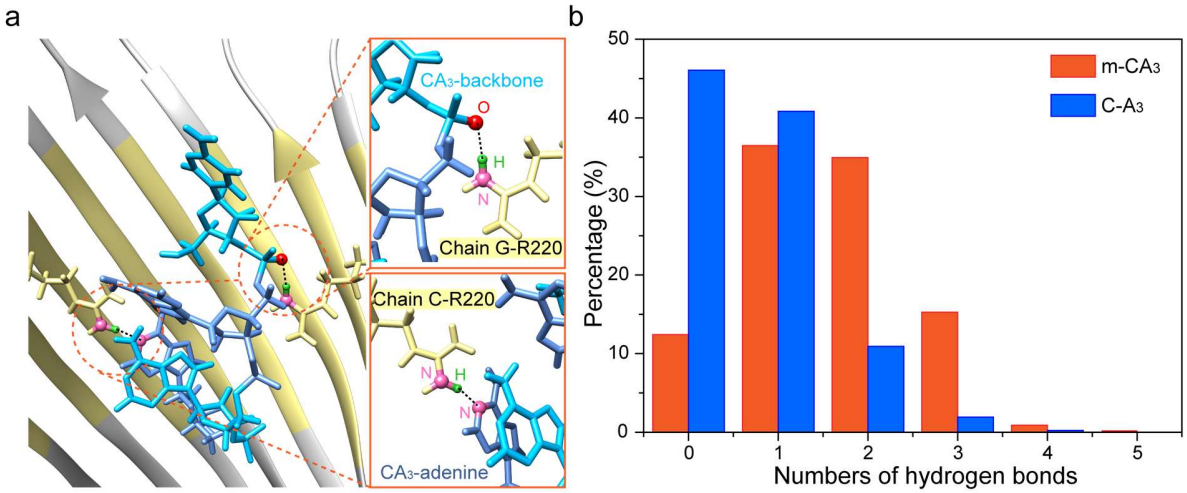

Figure S10 Comparison of hydrogen bonds between mC-A_3 (red) or C-A_3 (blue) with R1 region of the WT aerolysin protein. (**a**) Example of hydrogen bonds formed between C-A_3 and amino acid residues in R1 region. The atoms that formed hydrogen bonds were drawn as ball module while the other part of oligonucleotide and residues were drawn as stick bonds. The black dash line represents the hydrogen bonds. (**b**) The percentage of numbers of hydrogen bonds between mC-A_3 (red) or C-A_3 (blue) and R1 region found in the frames from last 10-ns simulation. The zero value for the number of hydrogen bonds represents that no hydrogen bonds were founded between the oligonucleotides and R1 region. The hydrogen bonds were determined according to the geometry criterion, in which the H···A distance was shorter than 3.0 Å and the H-D···A angle was lower than 20 degrees. The hydrogen bonds forming between the two oligonucleotides and amino acid residues in R1 region are counted in each frame from the last 10-ns MD simulation.

Table S3. Hydrogen bonds between the two oligonucleotides and amino acid residues in R1 region of aerolysin.

Hydrogen bonds	Occupancy (%)	
	mC-A_3	C-A_3
R220-DNA	115.26	61.02
T274-DNA	37.13	0
T218-DNA	0.82	0.02
S278-DNA	2.19	6.49

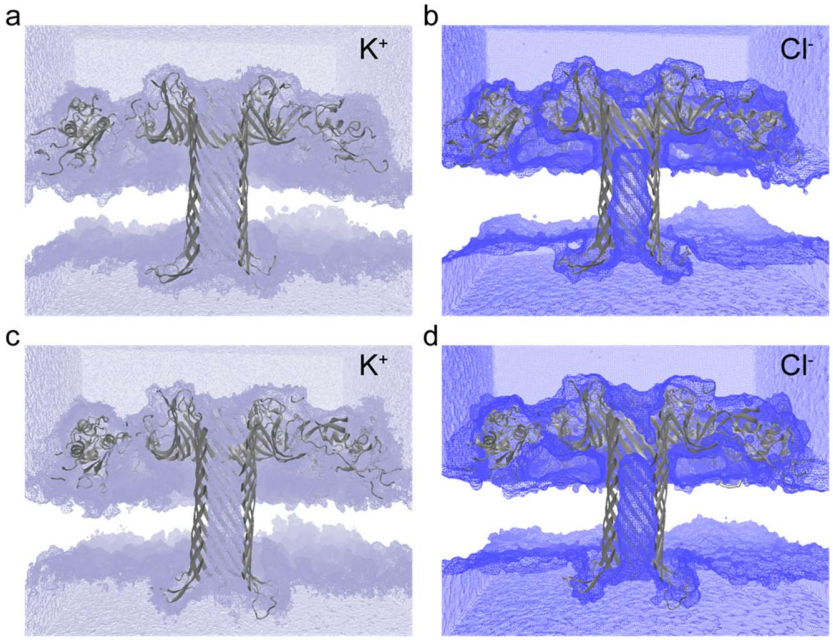

Figure S11. The ion density for C-A_3 and mC-A_3 inside aerolysin. (a)-(b) The density of K^+ (a) and Cl^- (b) for C-A_3 inside aerolysin during the 20-ns simulation under the applied voltage of +120 mV. (c)-(d) The density of K^+ (c) and Cl^- (d) for mC-A_3 inside aerolysin during the 20-ns simulation under the applied voltage of +120 mV. The ion density was calculated using VolMap plugin with the radiuses of K^+ and Cl^- was set to 0.95 Å and 1.81 Å, respectively.

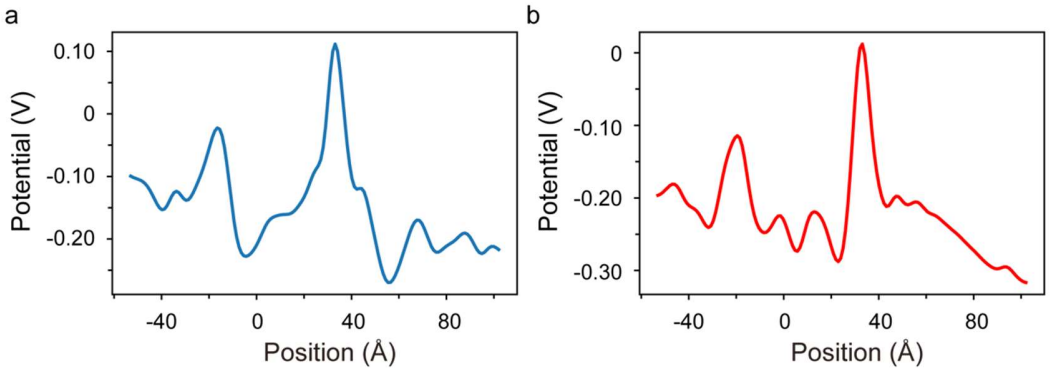

Figure S12. The electrostatistic potential along with the aerolysin lumen with C-A_3 (a) and mC-A_3 (b) located in R1 region under the applied voltage of +120 mV. The potential was calculated using PMEPot Plugin according to the previous work[3] based on the last 1.0-ns simulation trajectories.

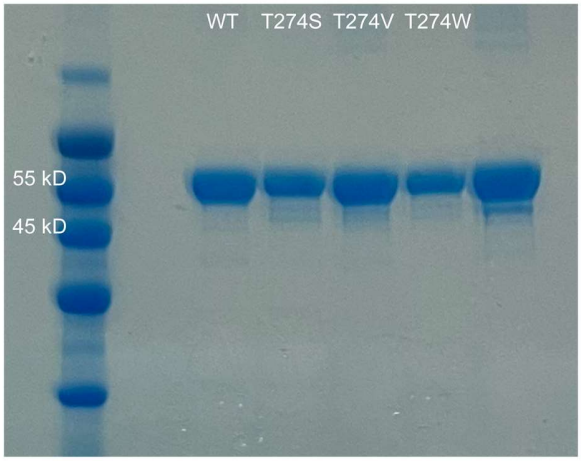

Figure S13. SDS-PAGE analysis of WT, T274S, T274V and T274W mutant proaerolysin.

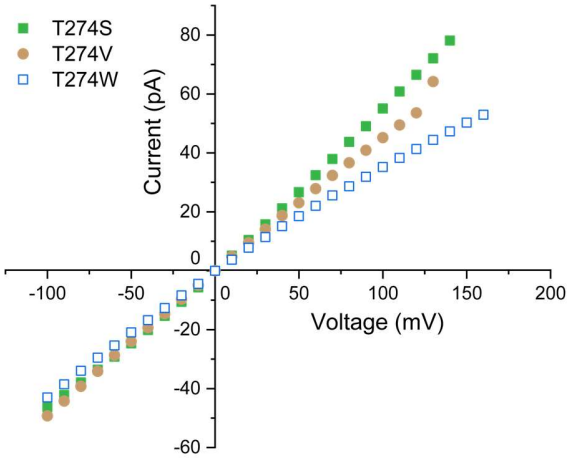

Figure S14. I-V curve of T274S, T274V and T274W mutant aerolysin nanopore. The data were aquired in 1.0 M KCl, 10 mM Tris, 1.0 mM EDTA with pH = 8.0 at 20 ± 2 ℃.

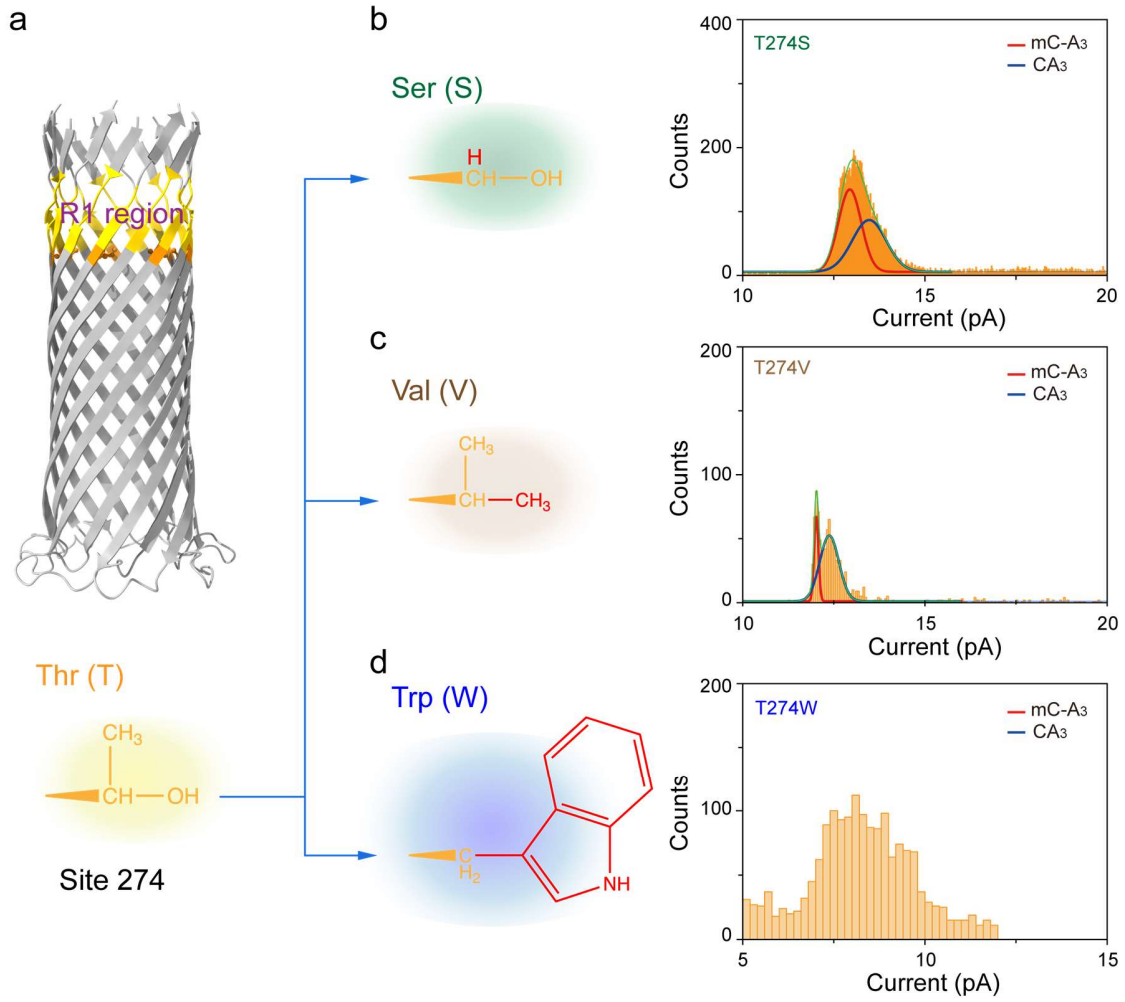

Figure S15. The discrimination of mC-A_3 and C-A_3 in T274S, T274V and T274W mutant aerolysin. (a) Illustration of Thr (T) at 274 site in R1 region. (b)-(d) *Left:* The chemical structures of serine (b), valine (c) and tryptophan (d); *Right*: The histrogram of residual current for the miture of mC-A_3 and C-A_3 in T274S (b), T274V (c) and T274W (d) mutant aerolysin nanopore. All data were acquired in 1.0 M KCl, 10 mM Tris, and 1.0 mM EDTA, pH 8.0, 20 ± 2 ℃ at the applied voltage of +60 mV in the presence of 2.0 μM mC-A_3 and C-A_3.

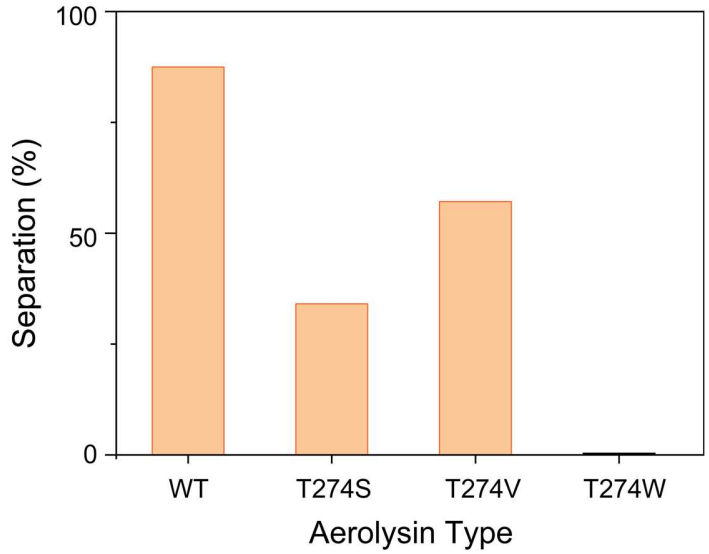

Figure S16. The separation of the two current peaks corresponding to mC-A_3 and C-A_3 in WT, T274S, T274V and T274W mutant aerolysin nanopore. All data were acquired in 1.0 M KCl, 10 mM Tris, and 1.0 mM EDTA, pH 8.0, 20 ± 2 ℃ at the applied voltage of +60 mV in the presence of 2.0 μM mC-A_3 and C-A_3.

Reference:

1. Hu, Z., Li, Z., Ying, Y., Zhang, J., Cao, C., Long, Y., Tian, H. Real-Time and Accurate Identification of Single Oligonucleotide Photoisomers via an Aerolysin Nanopore. *Anal. Chem.* **2018**, *90*, 4268-4272.

2. Smart, O. S., Neduvelil, J. G., Wang, X., Wallace, B. A., Sansom, M. S. P. HOLE: A Program for the Analysis of the Pore Dimensions of Ion Channel Structural Models. *J. Mol. Graphics* **1996**, *14*, 354–360.

3. Aksimentiev, A., Schulten, K. Imaging α-Hemolysin with Molecular Dynamics: Ionic Conductance, Osmotic Permeability, and the Electrostatic Potential Map. *Biophys. J.* **2005**, *88*, 3745–3761.